Metal-organic framework templated electrodeposition of functional gold nanostructures

CrossMark

Stephen D. Worrall[a,b], Mark A. Bissett[c], Patrick I. Hill[d], Aidan P. Rooney[c], Sarah J. Haigh[c], Martin P. Attfield[a,b,*], Robert A.W. Dryfe[b,*]

[a] Centre for Nanoporous Materials, School of Chemistry, The University of Manchester, Oxford Road, Manchester, M13 9PL, United Kingdom
[b] School of Chemistry, The University of Manchester, Oxford Road, Manchester, M13 9PL, United Kingdom
[c] School of Materials, The University of Manchester, Oxford Road, Manchester, M13 9PL, United Kingdom
[d] School of Chemical Engineering and Analytical Science, The University of Manchester, Oxford Road, Manchester, M13 9PL, United Kingdom

A B S T R A C T

Utilizing a pair of quick, scalable electrochemical processes, the permanently porous MOF HKUST-1 was electrochemically grown on a copper electrode and this HKUST-1-coated electrode was used to template electrodeposition of a gold nanostructure within the pore network of the MOF. Transmission electron microscopy demonstrates that a proportion of the gold nanostructures exhibit structural features replicating the pore space of this ∼1.4 nm maximum pore diameter MOF, as well as regions that are larger in size. Scanning electron microscopy shows that the electrodeposited gold nanostructure, produced under certain conditions of synthesis and template removal, is sufficiently inter-grown and mechanically robust to retain the octahedral morphology of the HKUST-1 template crystals. The functionality of the gold nanostructure within the crystalline HKUST-1 was demonstrated through the surface enhanced Raman spectroscopic (SERS) detection of 4-fluorothiophenol at concentrations as low as 1 μM. The reported process is confirmed as a viable electrodeposition method for obtaining functional, accessible metal nanostructures encapsulated within MOF crystals.

© 2016 The Authors. Published by Elsevier Ltd. This is an open access article under the CC BY license (http://creativecommons.org/licenses/by/4.0/).

1. Introduction

Metal-organic frameworks (MOFs) are a well-established family of nanoporous material whose framework is constructed from metal based inorganic clusters connected by heteroatom-containing organic linker molecules. MOFs have been investigated for a diverse range of applications [1]. Although they exhibit excellent properties for many of these applications in their pure form, the inclusion of MOFs as components in composite materials has provided many new exciting opportunities for their application in other areas [2].

The encapsulation of nanostructures within preformed MOF crystals [3], or during MOF crystal growth [4], have been demonstrated to be very effective methods to obtain composites with exciting properties [2]. A diverse range of nanostructured materials, including nanostructured carbon [5], polymer [6], metal hydride [7], polyoxometalate [8], metal oxide [9], metal nitride [10] and metal [11], have been incorporated into individual, or aggregates of, MOF crystals. A diverse range of different techniques have been employed in the synthesis of a variety of different encapsulated nanostructured metal/MOF composites [12–19], for application in areas such as substrates for surface enhanced Raman spectroscopy (SERS) [12] and catalysis [16–18]. A particularly elegant example of a truly MOF-templated metal nanostructure appears to be that reported by Volosskiy et al. [19] These workers used a judicious choice of solvent/reducing agent to synthesize ∼3 nm diameter Au and Pd nanowires that appear to be truly templated by the one dimensional ∼3 nm diameter pores of MOF-545.

Amongst the wide variety of different techniques utilized to obtain encapsulated nanostructured metal/MOF composites, electrodeposition stands out, surprisingly, as being the least developed. Electrodeposition should have the advantage over other techniques for the deposition of nanostructures within MOF pore structures due to its ability to plate topologically demanding nanoscale features [20]. To the best of the authors' knowledge, there has been only one report of the use of electrodeposition to

obtain a metal/MOF composite that involved forming metal sheets by electroreduction and agglomeration of the constituent metal ions of the layered MOF. This electrodeposition process involved destruction of the MOF itself [13]. Limited evidence for the presence of metal sheets on the external surface of the remaining MOF crystallites was provided for this poorly characterized metal/MOF composite formed by a non-templated electrodeposition process. On the contrary, templated electrodeposition has been successfully utilized to prepare composites of encapsulated metal nanostructures within other porous materials including anodized alumina [21], mesoporous silica [22], and hierarchical mesoporous silica/anodized alumina [23]. Aligned arrays of ~350 nm long and ~65 nm diameter Au nano-rods were fabricated within large pore anodized alumina[21] and much thinner, ~7 nm diameter and hundreds of nm long, Pd nanowires were produced by encapsulation within smaller pore diameter mesoporous silica [22]. It has also been shown that a supercritical fluid based electrolyte can be used with mesoporous silica coatings to template the electrodeposition of ~3 nm diameter Cu nanowires [20]. The random nature of the pores of the mesoporous silica resulted in relatively poor alignment of the nanowires[22] in contrast to those formed in the well aligned pores of the anodized alumina [21]. Subsequently, these two porous materials were combined to achieve the templated electrodeposition of well aligned nanowires, ~10 nm in diameter and hundreds of nm long, of Ag, Cu and Te [23]. Nanoporous MOFs have the potential to provide a similar combination of ordered porosity, matched with an even smaller pore size, yielding the potential to electrodeposit nanostructures with minimum dimensions of <2 nm embedded in a porous material. Previous work using nanoporous zeolites as templates for electrodeposition reported the formation of isolated metal nanoparticles only within the pore structures rather than extended nanostructures, with no precise determination of the deposited metal particle size or distribution [24].

In order to utilize MOFs for templated electrodeposition they must be attached to an electrode surface as a single crystal or a well intergrown coating of crystals. One method to achieve the latter is the electrochemical anodic dissolution method, whereby a well intergrown coating of MOF crystals is formed directly on the surface of a metal anode by the application of a potential between two metal electrodes, of the metal of the desired MOF, immersed in an electrolyte solution containing the organic linker of the desired MOF [25]. The resultant MOF crystals provide for a relatively continuous and defect free coating that has the added advantage of being strongly adhered to the electrode surface [26]. A variety of carboxylate and imidazole-based MOF coatings have been formed using this route [25–30] including the archetypal copper trimesate MOF, HKUST-1 $Cu_3[C_6H_3(CO_2)_3]_2(H_2O)_3$ [31]. HKUST-1 is assembled from $Cu_2(H_2O)_2$ dimer units and tridentate trimesate (benzene-1,3,5-tricarboxylate) groups to form a three-dimensional framework structure containing a three-dimensional channel system. The channels consist of alternating cavities of ~1.4 nm pore diameter and ~1.1 nm pore diameter connected through pores of ~1.0 nm diameter as shown in Fig. 1 [32]. There are also smaller ~0.5 nm diameter cavities present in the structure between the larger cavities.

In this work we demonstrate for the first time that a porous MOF, HKUST-1, can be used successfully to template electrodeposition of a metal, gold, nanostructure within the pore network of the MOF and that a proportion of the nanostructures exhibit structural features replicating the pore space of the MOF. The high surface area, rough nature of the HKUST-1 encapsulated gold nanostructure is shown to act as an ideal surface enhanced Raman spectroscopic (SERS) substrate.
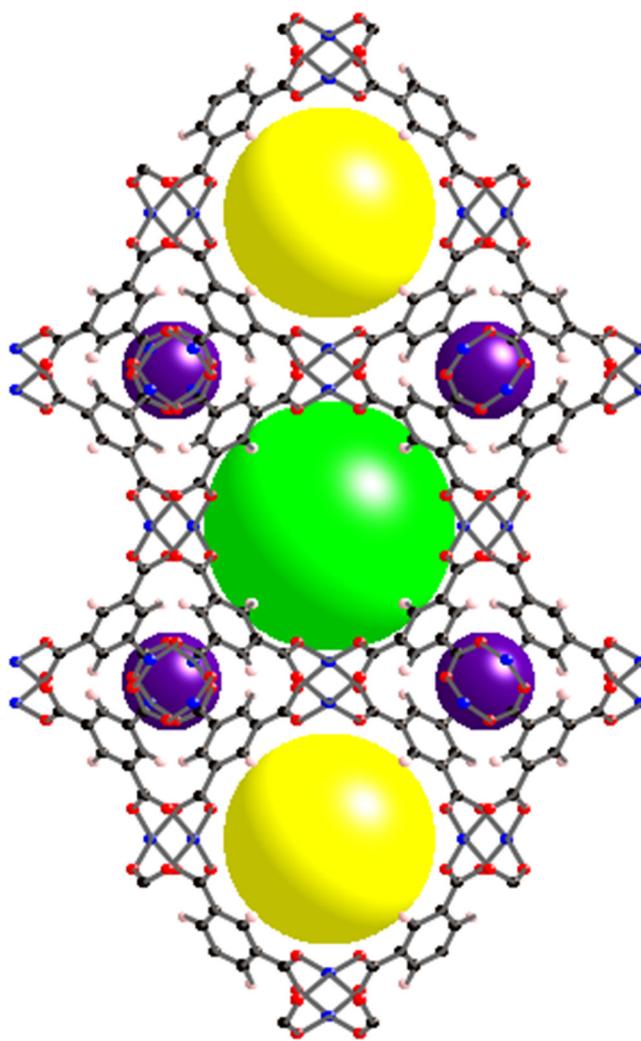
Fig. 1. Structure of HKUST-1 displaying the cavities of ~1.4 nm pore diameter (green sphere), ~1.1 nm pore diameter (yellow sphere) and ~0.5 nm diameter (purple sphere). Key Cu − blue, O − red, C − black, H − pink. (For interpretation of the references to colour in this figure legend, the reader is referred to the web version of this article.)

2. Experimental

2.1. Materials

Cu foil (oxygen free high conductivity), 4-fluorothiophenol (98 +%) and sodium tetrachloroaurate dihydrate NaAuCl$_4$·2H$_2$O (99.99%) were obtained from Alfa Aesar. Hydrochloric acid HCl (37%) and hydrogen peroxide H$_2$O$_2$ (30%) were obtained from Fisher Scientific. Repro rubber (thin pour) was obtained from Flexbar. Tetrabutylammonium chloride TBACl (99%) was obtained from Fluka. Deionized water (18.2 MΩ cm) was obtained from a Milli-Q Millipore Direct 8 purification unit. 1,3,5-benzenetricarboxylic acid BTC (95%), dimethyl sulfoxide DMSO (≥99.9%), ethanol (≥99.8%), methanol (≥99.9%) and methyltributylammonium methyl sulfate MTBAMS (≥95%) were obtained from Sigma Aldrich.

2.2. HKUST-1 coating synthesis

Two Cu foil electrodes (each ~16 cm^2) were coated on one side with Repro rubber, which was left to set, rendering that side electro-chemically inactive. The Repro rubber coated Cu foil electrodes were then immersed, active sides face to face and ~2 cm

apart, in a solution of 48 mM BTC and 64 mM MTBAMS in 1:1 ethanol:H$_2$O and heated to 55 °C. N$_2$(g) was bubbled into the solution throughout the synthesis. A PGSTAT302N Potentiostat (Metrohm Autolab B. V., The Netherlands) was used to apply a fixed potential difference of 2.5 V between the two Repro rubber coated Cu foil electrodes for 30 minutes. The HKUST-1 coated anode was removed from the growth solution and rinsed three times with methanol to remove residual linker and supporting electrolyte. HKUST-1 was also formed in solution during the synthesis but this material was discarded.

2.3. HKUST-1 templated Au electrodeposition

A HKUST-1 (front) and Repro rubber (back) coated Cu foil working electrode, carbon rod counter electrode and Ag wire "pseudo" reference electrode were immersed in a solution of 10 mM NaAuCl$_4$·2H$_2$O and 0.1 M TBACl in DMSO. Au electrodeposition was performed under both potentiostatic and potentiodynamic conditions in order to yield Au/HKUST-1. Potentiostatic electrodeposition was performed by application of −1.2 V vs Ag for 30 minutes. Potentiodynamic electrodeposition was performed by cycling the applied potential between −0.2 V and −1.3 V vs Ag, at 100 mV s^{-1} for 100 cycles. After the potential was removed the electrodes were rinsed three times with methanol to removed residual Au salt, supporting electrolyte and solvent.

2.4. Etching of HKUST-1 from Au/HKUST-1

Au/HKUST-1 was mechanically removed from the Cu foil electrode surface before the HKUST-1 template was etched away with the sequential use of deionized water, 1 M HCl (aq), deionized water, 5% H$_2$O$_2$ (aq), deionized water and, finally, methanol to yield the deposited Au. This process was done in one of two ways. In the first method a small amount of Au/HKUST-1 was immobilized onto an SEM stub and each successive wash solution was pipetted onto the stub, left for 10 minutes and then drawn off using adsorbent Kimwipes. This process was then repeated for each of the wash solutions. In the second method a larger amount of material was dispersed with sonication in a wash solution and left to stand for at least 10 minutes and until any bubbling had stopped. Centrifugation was then used to retrieve the Au/HKUST-1 before repeating the process with the next wash solution.

2.5. Exposing HKUST-1 to 4-fluorothiophenol

Au/HKUST-1 was mechanically removed from the Cu foil electrode surface and placed into a x mM solution of 4-fluorothiophenol in ethanol for 24 hours, where x = 1 µM − 2 mM. Au/HKUST-1 was then retrieved by filtration and washed repeatedly with ethanol before leaving to dry.

### 2.6. Characterisation of HKUST-1, Au/HKUST-1 and deposited Au

Powder X-ray diffraction (PXRD) was performed using a PANalytical X'Pert X-ray diffractometer using Cu-Kα radiation at 40 kV and 30 mA, in the range 5–60 2θ° (with a step size of 0.017 2θ° and scan step time of 66 s) with spinning of the sample. Confocal Raman spectroscopy was performed using a Renishaw inVia microscope with a 633 nm (1.96 eV) excitation, at a power of 1 mW, with a 100 x objective, to give a 1 µm spot size, and a grating of 1800 l mm^{-1} to achieve a spectral resolution of 1 cm^{-1}. Spectra shown are the average of 10 sets of 10 s exposures. Scanning electron microscopy (SEM) imaging − energy dispersive X-ray spectroscopy (EDS) was performed using a tandem FEI Quanta 200 (Environmental) Scanning Electron Microscope ((E)SEM) with an attached EDAX Genesis spectrometer. SEM images were obtained

at 20 kV under low vacuum with a water vapor pressure of 0.83 Torr utilizing a backscattered electron detector. EDS analysis was performed with a 132 eV resolution, a spot size of approximately 1 µm and 50 s collection time. All samples were stirred overnight in methanol before EDS analysis to remove DMSO due to the S Kα and Au M signals overlapping. X-ray photoelectron spectroscopy (XPS) was performed on a Kratos Axis Nova XPS spectrometer. Spectra were obtained using a high power monochromated Al-Kα source using the smallest available spot size of 10 µm diameter. Depth profiling was performed using an Ar ion gun in "normal mode" (5 kV V$_{SOURCE}$, 5 mA i$_{EMISSION}$ and 2.5 µA i$_{EXTRACTOR}$) and compucentric rotation. Transmission electron microscopy (TEM) bright field imaging was completed using a FEI Tecnai F30 operating at 300 kV. Samples were dispersed in methanol with 15 minutes sonication at full power and pipetted onto 200 mesh Cu holey carbon grids and dried prior to imaging. Particle size analysis was performed using ImageJ, with images scaled, despeckled and background corrected before thresholding. Particle size analysis was performed with no filtering based on circularity, but with particles with an area less than 1 nm^2 excluded to eliminate artefacts.

3. Results and Discussion

3.1. Characterisation of HKUST-1 electrodes pre- and post-Au electrodeposition

The powder X-ray diffraction (PXRD) patterns of the HKUST-1 coated Cu foil before and after Au electrodeposition are shown in Fig. 2 and show that both potentiostatic and potentiodynamic deposition techniques resulted in the reduction of Au^{3+} to Au metal. The slightly greater intensity of the Au diffraction peaks relative to the HKUST-1 diffraction peaks in the sample produced by potentiostatic deposition can be attributed to the fact that Au electrodeposition is performed for a longer time (30 minutes) potentiostatically than potentiodynamically (18 minutes). The far larger full widths at half maxima of the Au diffraction peaks in comparison to those derived from the HKUST-1 template indicate that the sizes of the crystalline domains of the Au are of the order of nanometers. The presence of Cu$_2$O in the as-grown HKUST-1 coated Cu foil is to be expected as the synthesis relies on the
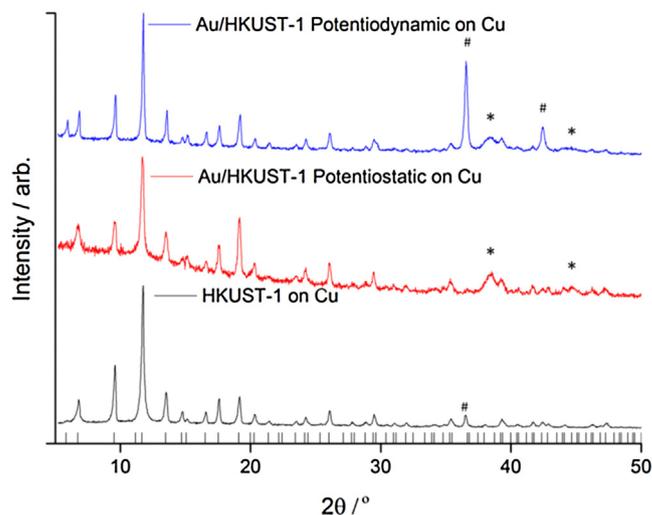
Fig. 2. PXRD patterns of HKUST-1 coated Cu foil before and after potentiostatic and potentiodynamic Au electrodeposition respectively (see Experimental section). Peaks marked with * are assigned to Au [40] and those marked with # are assigned to Cu$_2$O [41]. The vertical black lines along the x axis denote the predicted peak positions for HKUST-1 [31].

oxidation of the Cu foil [25]. The extremely low abundance of Cu_2O present in the potentiostatically deposited Au sample results from the magnitude of the potential applied in this procedure that is sufficient to reduce Cu_2O to Cu. The increased presence of Cu_2O after potentiodynamic deposition can be attributed to the fact that a potential sufficient to oxidize Cu is applied for a portion of each cycle of the potentiodynamic process. Additionally it could also result from a galvanic displacement reaction occurring between the Au^{3+} ions in solution and the underlying Cu electrode during the portions of the cycle where the applied potential is insufficient to reduce Au^{3+} to Au.

The Raman spectra of the HKUST-1 coated Cu foil pre- and post-Au electrodeposition are shown in Fig. 3 and show no significant differences. This is expected as Au is not Raman active. Slight variations in the relative peak intensities and positions can however be attributed to the presence of the Au which selectively enhances certain vibrations within the HKUST-1 framework [33].

Example scanning electron microscopy (SEM) images of HKUST-1 coated Cu foil pre- and post-Au electrodeposition are shown in Fig. 4. The left hand image of the HKUST-1 coated Cu foil before electrodeposition shows a good coverage of predominantly octahedral HKUST-1 crystals all over the surface. The absence of brighter areas derived from exposed underlying Cu metal demonstrates that any defects in the coating must be too small to be resolved by the SEM. The bright areas in the backscattered SEM images of the HKUST-1 coated Cu foil after both potentiostatic and potentiodynamic electrodeposition indicate the presence of exposed metal, which is confirmed as deposited Au by energy dispersive X-ray spectroscopy (EDS) as shown in Fig. 5. The
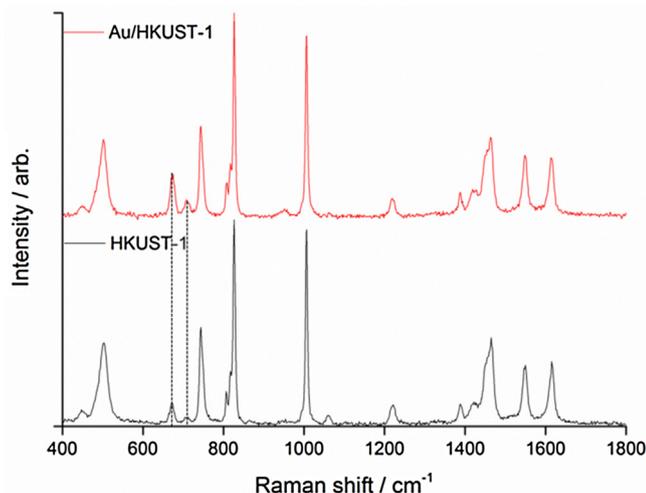
presence of this "bulk" gold is ascribed to the presence of nanoscale defects in the HKUST-1 coating that were not observable using SEM imaging. Such defects provide a preferable diffusion pathway for the solvated Au^{3+} precursor ions to reach the underlying Cu foil, so bypassing the pore network of the HKUST-1 crystals. More interestingly, the EDS spectra taken in locations where no visible surface Au was present also exhibit a signal for Au (Fig. 5). This indicates that Au has been deposited through the HKUST-1 framework and is not confined to defects in the coating. The absence of a signal for Au in a sample of HKUST-1 powder exposed to the Au electrodeposition solution without application of a potential (see Fig. 5) confirms that the observed Au signal in the Au/HKUST-1 composite coatings is due to electrodeposited Au rather than Au^{3+} ions trapped in the pores.

X-ray photoelectron spectroscopy (XPS) depth profiling was used to assess the distribution of the deposited Au through the HKUST-1 coating on the electrode as shown in Fig. 6. The Au XPS signal increased with increasing etch time which is consistent with the hypothesized Au electrodeposition process occurring through a template that starts at the underlying electrode surface before growing up through the template. The individual XPS spectra contributing to Fig. 6 are provided in Figure A1.

The presence of the Au deposited in the HKUST-1 framework was confirmed using transmission electron microscope (TEM) imaging of the Au/HKUST-1 composites obtained by both potentiostatic and potentiodynamic electrodeposition. Anisotropic Au nanostructures deposited via both electrodeposition methods can be observed to be embedded within the HKUST-1 framework in Fig. 7. Those obtained from potentiostatic deposition (Fig. 7A) range in smallest dimension from $\sim$1.1–4.2 nm ($d_{MEAN} \sim$ 1.8 nm) whilst those obtained from potentiodynamic deposition (Fig. 7B) are slightly larger, ranging in diameter from $\sim$1.2–4.6 nm ($d_{MEAN} \sim$2.5 nm) and are less densely distributed within the framework. This slight variation can be attributed to the difference in the deposition techniques. In the case of potentiostatic deposition the constant application of a potential sufficient to reduce Au^{3+} to Au would lead to a constantly high rate of nucleation and growth, hence the more densely distributed and smaller anisotropic nanostructures. In contrast, for a significant proportion of the time during potentiodynamic deposition the applied potential is insufficient to reduce Au^{3+} to Au. This would lead to a lower rate of nucleation and growth and potentially explain the less densely distributed and slightly larger anisotropic nanostructures that form as a result. The average smallest dimension of the anisotropic nanostructures synthesized by both methods is greater than that of the largest pore diameter of the HKUST-1 template $\sim$ 1.4 nm [32]. However, the size distributions (see Figure A2) show that, whilst the anisotropic nanostructures display a wide range of smallest dimensions, a proportion of them are smaller in size than the diameter of the largest HKUST-1 pore [32]. This is particularly noticeable in the case of the anisotropic nanostructures synthesized potentiostatically, where anisotropic nanostructures with

Fig. 3. The Raman spectra of HKUST-1 coated Cu foil pre- and post-Au electrodeposition (see Experimental section). The peaks slightly enhanced in the Au/HKUST-1 composite are marked with dashed lines.
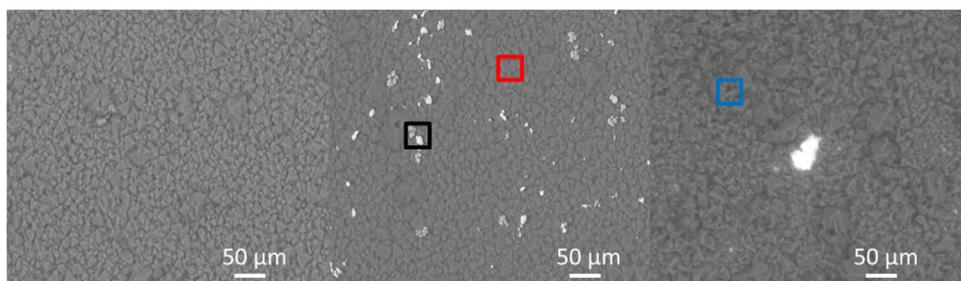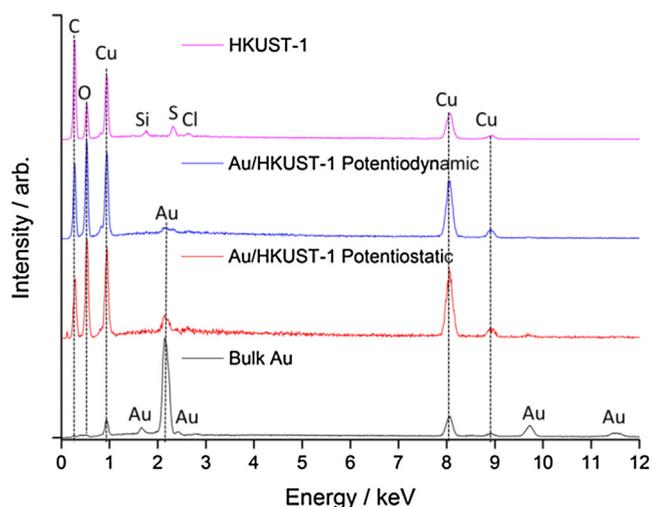

Fig. 4. Backscattered electron SEM images of $\sim$ 10 μm thick coatings of HKUST-1 on Cu foil pre- (left) and post-Au electrodeposition using potentiostatic (middle) and potentiodynamic (right) conditions respectively (see Experimental section).

Fig. 5. Comparison of EDS spectra for bulk Au deposits, Au/HKUST-1 composites and powder HKUST-1 exposed to the Au electrodeposition solution overnight without any applied potential (see Experimental section). The bulk Au spectrum, the potentiostatically deposited Au/HKUST-1 spectrum and the potentiodynamically deposited Au/HKUST-1 spectrum were measured from the areas highlighted in black, red and blue in Fig. 4 respectively. (For interpretation of the references to colour in this figure legend, the reader is referred to the web version of this article.)
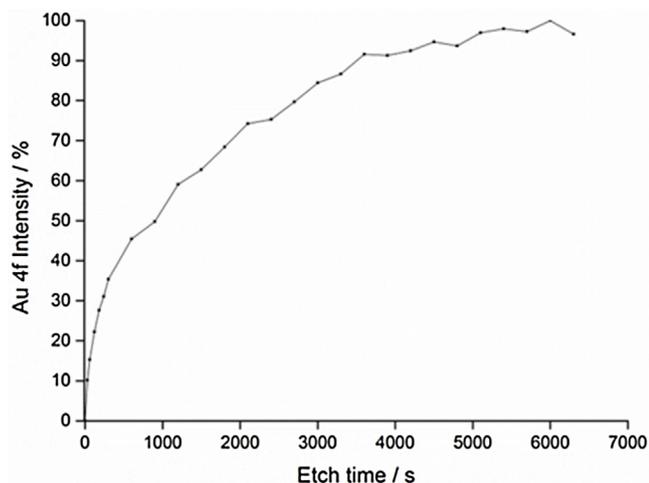
Fig. 6. XPS depth profile of the Au 4f signal of a potentiostatically deposited Au/HKUST-1 sample.
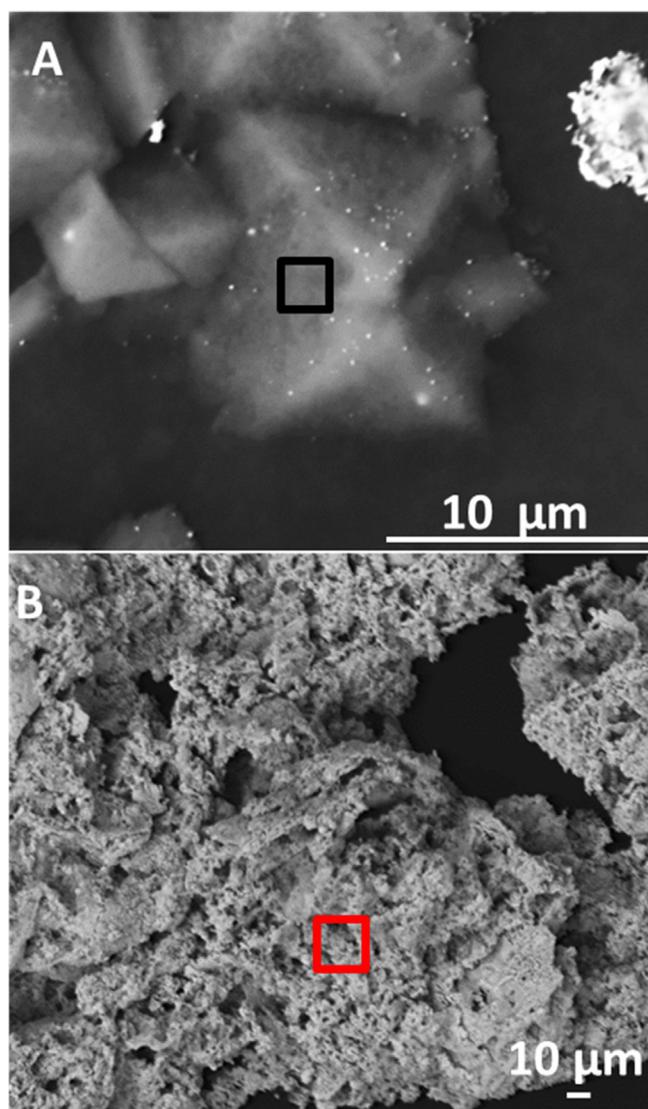
smallest dimensions <2 nm dominate with over a third being smaller in size than the diameter of the largest HKUST-1 pore [32]. The possibility that isolated nanoparticles were able to nucleate away from the underlying electrode surface within the highly resistive HKUST-1 framework[34] cannot be definitively discounted because the 2D cross sectional images provided by TEM do not give any information on the geometry of the observed nanostructures out of the plane. The results suggest that HKUST-1 is capable of templating the growth of anisotropic Au nanostructures that are replicas of components of the pore space within the MOF during electrodeposition, but that the framework of HKUST-1 is not strong enough to prevent the growth of the anisotropic nanostructures that have sizes greater than the largest pore diameter of the framework. Similar rupture of MOF pores using chemical techniques for depositing metals inside MOF structures has been reported [35].
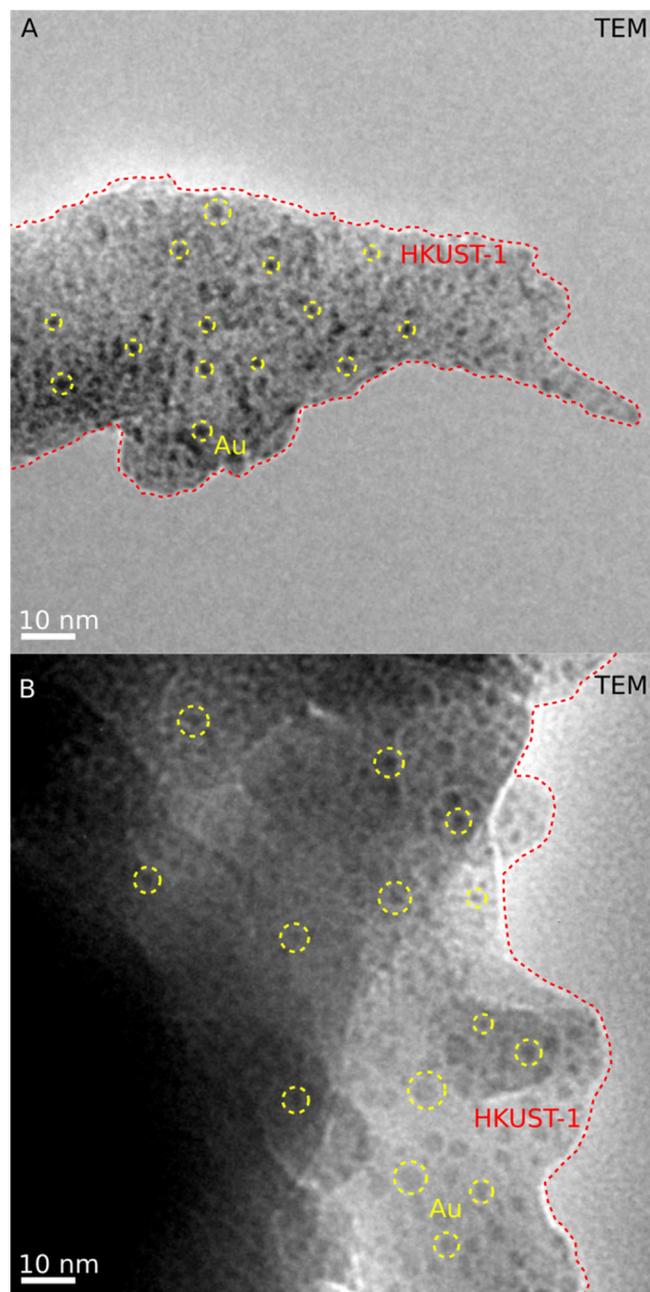
Fig. 7. Bright field TEM images of Au/HKUST-1 composites obtained by potentiostatic (A) and potentiodynamic (B) Au electrodeposition (see Experimental section). HKUST-1 area highlighted in red and anisotropic Au nanostructures highlighted in yellow. (For interpretation of the references to colour in this figure legend, the reader is referred to the web version of this article.)

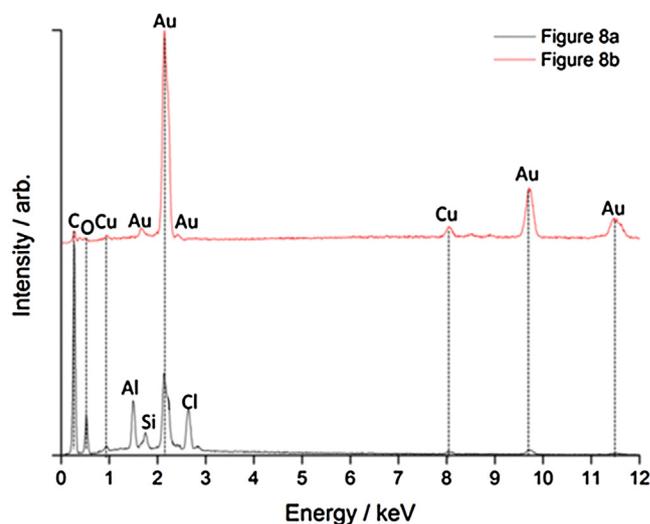### 3.2. Characterisation of electrodeposited Au post HKUST-1 removal

As the potentiostatically deposited Au/HKUST-1 composite displayed anisotropic Au nanostructures with smaller dimensions it was subjected to an etching process to remove the HKUST-1 to allow further characterization of the Au. PXRD patterns of the Au demonstrate that the etching process, when performed in solution, effectively removes the HKUST-1 template as the only diffraction peaks observed are those of crystalline Au (see Figure A3). SEM images of the deposited Au are shown in Fig. 8 alongside the corresponding EDS spectra in Fig. 9. If the etching process was performed in situ on the SEM stub then it was possible to obtain images such as that shown in Fig. 8a where the original octahedral

Fig. 8. Backscattered electron SEM images of deposited Au obtained after etching away the HKUST-1 template *in situ* (A) or in solution (B) (see Experimental section).
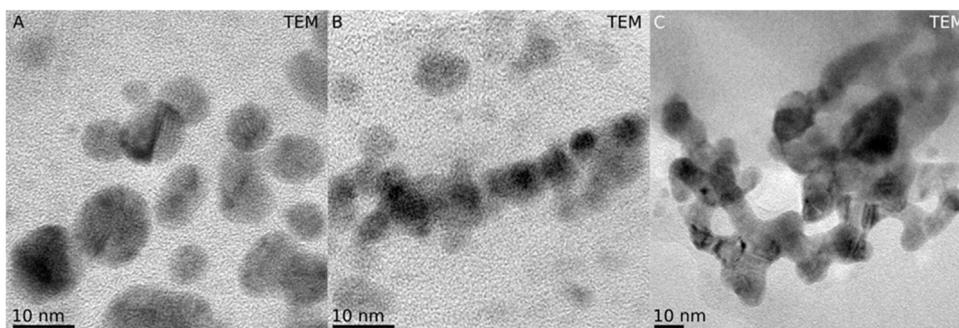

Fig. 9. EDS spectra of deposited Au obtained by etching away the HKUST-1 template (see Experimental section). The black (bottom) spectra was taken in the black rectangle in Fig. 8a and the red (top) spectra was taken in the red rectangle in Fig. 8b. (For interpretation of the references to colour in this figure legend, the reader is referred to the web version of this article.)

obtained show that the aggregate observed in Fig. 8b is composed of Au nanoparticles with a range of sizes (see Fig. 10a), short nanowires (see Fig. 10b) and more complex structures (see Fig. 10c). The diameters of the observed nanoparticles are greater than the smallest dimensions of the anisotropic nanostructures embedded within the HKUST-1 framework. This could possibly be due to the etching process leaving a residual carbonaceous coating on the nanoparticles which contributes to their observed dimensions or it could be due to the uncapped Au nanoparticles undergoing Ostwald ripening once the HKUST-1 template is removed and no longer immobilizes them [36]. In a more pertinent example Wang et al. [22] observed, via PXRD, evidence of aggregation of the metallic nanostructures they had electro-deposited within mesoporous silica once the template was removed. The presence of anisotropic nanostructures is to be expected given the pore structure of HKUST-1 and the likely anisotropic growth of the Au nanostructures through the MOF template. The observed isolated nanoparticles could be due to the sonication used to break up the aggregate also being sufficiently intense to break up the anisotropic nanostructures.

3.3. Electrodeposited Au/HKUST-1 composite as a SERS substrate

The potentiodynamically deposited Au/HKUST-1 composites were used as substrates for SERS. One of the myriad of applications reported for metal/MOF composites is their use as SERS substrates for the detection of small organic molecules [12,37,38]. The immobilized anisotropic Au metal nanostructures within the HKUST-1 pores provide an ideal high surface roughness substrate for SERS and the location of the metal within the MOF crystals precludes larger molecules from reaching the metal surface. In order to test whether the Au/HKUST-1 composites produced by electrodeposition were SERS active, 4-fluorothiophenol was used as a probe molecule. The peak with the greatest intensity in the Raman spectrum of bulk 4-fluorothiophenol occurs at 1098 cm^{-1} and arises from the vibration of the C-F bond. This peak downshifts by over 20 cm^{-1} to 1077 cm^{-1} when thiol binds to a gold surface [39].

Au/HKUST-1 samples were exposed to four different concentrations of 4-fluorothiophenol in ethanol (2 mM, 1 mM, 0.1 mM and 1 μM): the resultant Raman spectra can be seen in Fig. 11. At all four

morphology of the cubic HKUST-1 template is visible, despite the fact that the MOF template has been etched away, as evidenced by the very low Cu signal observed in the corresponding EDS spectrum (see Fig. 9). The high C, O and Si signals are attributed to the adhesive used to affix the sample to the SEM stub and the Cl signals are a result of the HCl (aq) used during the etching process reacting with the Al SEM stub. This indicates that in some cases the anisotropic Au nanostructures electrodeposited within the MOF are sufficiently interlinked so as to retain their original HKUST-1 template crystal morphology on removal of the MOF template. However, these structures are fragile because when the etching process is performed in solution, the SEM images of the deposited Au are represented by that shown in Fig. 8b where there is no indication that the original crystal habit of the HKUST-1 template is retained. The etching process is cleaner in this case, with only traces of elements other than Au observed in the EDS spectra (see Fig. 9). The deposit appears to be an aggregate of many smaller Au micro- and nanostructures, which is to be expected considering the solution based etching process utilizes centrifugation which would cause the deposited Au to agglomerate.

TEM was used in order to analyze the aggregates observed in Fig. 8b after sonication was used to break them up. The images

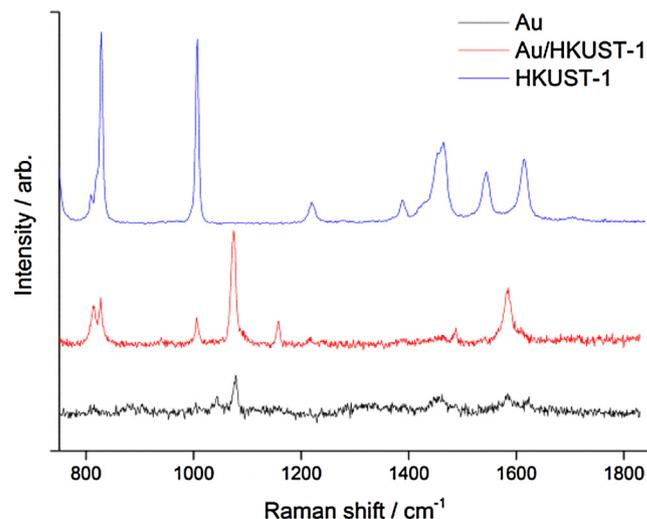**Fig. 10.** TEM images of potentiostatically deposited Au obtained by etching away of HKUST-1 template.
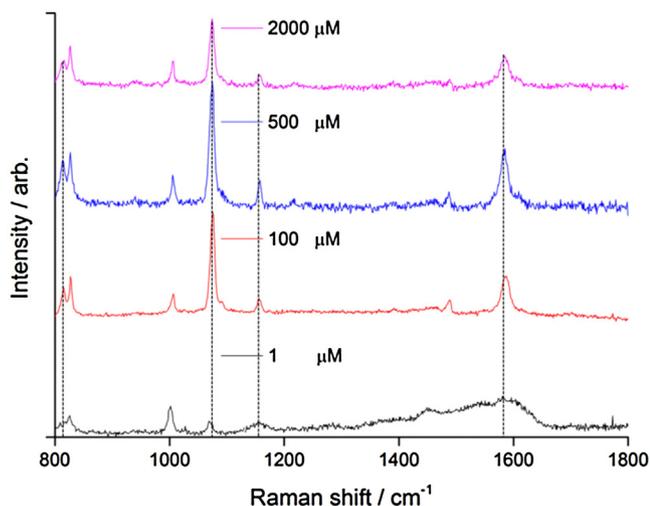
Fig. 11. Raman spectra of Au/HKUST-1 samples after exposure to different concentrations of 4-fluorothiophenol in ethanol. Marked peaks are those of 4-fluorothiophenol bound to Au, unmarked peaks are those of HKUST-1.


Fig. 12. Raman spectra of roughened Au foil (black), Au/HKUST-1 (red) and HKUST-1 (blue) after exposure to 2 mM 4-fluorothiophenol in ethanol. (For interpretation of the references to colour in this figure legend, the reader is referred to the web version of this article.)

concentrations, the peak at 1077 cm^{-1} corresponding to the C − F vibration of the molecule bound to Au is clearly visible. Observation of this shift in the Raman spectra demonstrates that the Au, rather than the HKUST-1 template, is responsible for the SERS effect as opposed to the MOF itself. This is further confirmed by exposing pure HKUST-1 samples to the same probe molecule concentrations as the Au/HKUST-1 samples with no observation of a signal for 4-fluorothiophenol (see Fig. 12 and Figure A4). The Au/HKUST-1 composite is also shown to be a superior SERS substrate for the detection of 4-fluorothiophenol than a roughened gold foil (see Fig. 12).

Additionally peaks at 814 cm^{-1} (C − H wagging), 1156 cm^{-1} (C − H in plane bending) and 1589 cm^{-1} (C − C stretching) are also apparent at all concentrations. This data shows that the Au/HKUST-1 composites prepared by electrodeposition are effective SERS substrates for the detection of 4-fluorothiophenol down to at least 1 μM, a concentration lower than that reported for any other Au/MOF composite [12,37]. Evidence that the signal originates from the Au/HKUST-1 composite, as opposed to a bulk Au deposit like those seen in Fig. 4, is confirmed with the demonstration that the signal can be observed within the triangular (111) facet of an individual HKUST-1 crystal (Figure A5).

An additional advantage of being able to observe this particular SERS effect is that it enables the distribution of Au within the Au/HKUST-1 composite to be analyzed utilizing Raman spectroscopy

mapping as can be seen in Fig. 13. By taking a series of 440 individual spectra in a raster pattern over the sample (see Appendix B for Raman map raw data), and then plotting the peak intensity at 1077 cm^{-1} as a function of that pattern, a map of 4-fluorothiophenol bound to Au is obtained. It is evident from the map that Au is not uniformly distributed throughout the HKUST-1 coating, and that there is a network of electrodeposited Au running through the sampled area.

4. Conclusions

In this work we have demonstrated that an electrochemically grown, electrode attached porous MOF can be used successfully as a template for the electrodeposition of extended metal nano-structures within the pore network of the MOF. A proportion of these metal nanostructures is truly templated by the pore space of the MOF and is demonstrated to function as a useful SERS substrate. Given that a variety of MOFs can be electrochemically grown on the surface of metal electrodes via anodic dissolution [27–30], MOF-templated electrodeposition is suggested as a viable route to obtain functional, accessible metal nanostructures encapsulated within MOF crystals.
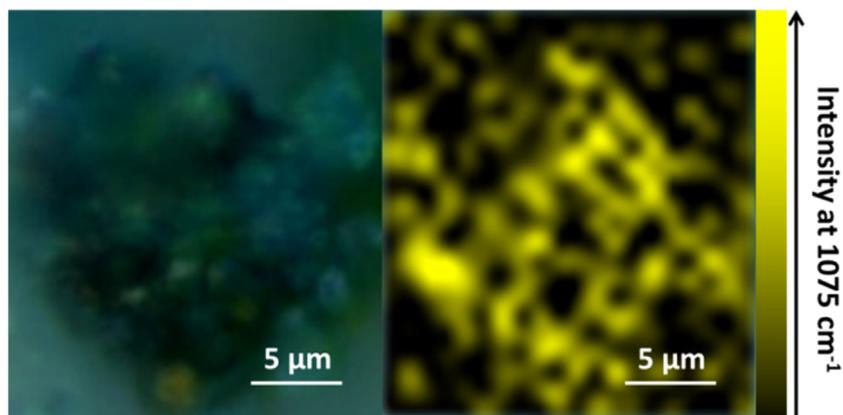
Fig. 13. Optical image (left) and corresponding Raman map (right) of an Au/HKUST-1 sample after exposure to 2000 μM 4-fluorothiophenol in ethanol.

Acknowledgements

Appendix A. Supplementary data

Supplementary data associated with this article can be found, in the online version, at http://dx.doi.org/10.1016/j.electacta.2016.10.187.

References

[1] H.-C. Zhou, S. Kitagawa, Metal – Organic Frameworks (MOFs), Chem. Soc. Rev. 43 (2014) 5415–5418.

[2] Q.-L. Zhu, Q. Xu, Metal-organic framework composites, Chem. Soc. Rev. 43 (2014) 5468–5512.

[3] T.T. Dang, Y. Zhu, J.S.Y. Ngiam, S.C. Ghosh, A. Chen, A.M. Seayad, Palladium Nanoparticles Supported on ZIF-8 As an Efficient Heterogeneous Catalyst for Aminocarbonylation, ACS Catal. 3 (2013) 1406–1410.

[4] X. Huang, B. Zheng, Z. Liu, C. Tan, J. Liu, B. Chen, H. Li, J. Chen, X. Zhang, Z. Fan, W. Zhang, Z. Guo, F. Huo, Y. Yang, L.-H. Xie, W. Huang, H. Zhang, Coating Two-Dimensional Nanomaterials with Metal–Organic Frameworks, ACS Nano 8 (2014) 8695–8701.

[5] H.L. Jiang, B. Liu, Y.Q. Lan, K. Kuratani, T. Akita, H. Shioyama, F.Q. Zong, Q. Xu, From Metal–Organic Framework to Nanoporous Carbon: Toward a Very High Surface Area and Hydrogen Uptake, J. Am. Chem. Soc. 133 (2011) 11854–11857.

[6] C. Lu, T. Ben, S. Xu, S. Qiu, Electrochemical Synthesis of a Microporous Conductive Polymer Based on a Metal–Organic Framework Thin Film, Angew. Chem. Int. Ed. 53 (2014) 6454–6458.

[7] R.K. Bhakta, J.L. Herberg, B. Jacobs, A. Highley, R. Ockwig, N.W. Behrens Jr., J.A. Greathouse, M.D. Allendorf, Metal-Organic Frameworks As Templates for Nanoscale NaAlH₄, J. Am. Chem. Soc. 131 (2009) 13198–13199.

[8] D. Mustafa, E. Breynaert, S.R. Bajpe, J.A. Martens, C.E.A. Kirschhock, Stability improvement of Cu₃(BTC)₂ metal-organic frameworks under steaming conditions by encapsulation of a Keggin polyoxometalate, Chem. Commun. 47 (2011) 8037–8039.

[9] A.S. Hall, A. Kondo, K. Maeda, T.E. Mallouk, Microporous Brookite-Phase Titania Made by Replication of a Metal–Organic Framework, J. Am. Chem. Soc. 135 (2013) 16276–16279.

[10] D. Esken, S. Turner, C. Wiktor, S.B. Kalidindi, G. Van Tendeloo, R.A. Fischer, GaN@ZIF-8: Selective Formation of Gallium Nitride Quantum Dots inside a Zinc Methylimidazolate Framework, J. Am. Chem. Soc. 133 (2011) 16370–16373.

[11] J.D. Evans, C.J. Sumby, C.J. Doonan, Post-synthetic metalation of metal-organic frameworks, Chem. Soc. Rev. 43 (2014) 5933–5951.

[12] K. Sugikawa, S. Nagata, Y. Furukawa, K. Kokado, K. Sada, Stable and Functional Gold Nanorod Composites with a Metal–Organic Framework Crystalline Shell, Chem. Mater. 25 (2013) 2565–2570.

[13] A. Domenech, H. Garcia, M.T. Domenech-Carbo, F. Llabres-i-Xamena, Electrochemistry nanometric patterning of MOF particles: Anisotropic

[14] M.P. Suh, H.R. Moon, E.Y. Lee, S.Y. Jang, A Redox-Active Two-Dimensional Coordination Polymer: Preparation of Silver and Gold Nanoparticles and Crystal Dynamics on Guest Removal, J. Am. Chem. Soc. 128 (2006) 4710–4718.

[15] R. Ameloot, M.B.J. Roeffaers, G. De Cremer, F. Vermoortele, J. Hofkens, B.F. Sels, D.E. De Vos, Metal–Organic Framework Single Crystals as Photoactive Matrices for the Generation of Metallic Microstructures, Adv. Mater. 23 (2011) 1788–1791.

[16] Y. Huang, Z. Lin, R. Cao, Palladium Nanoparticles Encapsulated in a Metal–Organic Framework as Efficient Heterogeneous Catalysts for Direct C2 Arylation of Indoles, Chem. Eur. J. 17 (2011) 12706–12712.

[17] H.-L. Jiang, B. Liu, T. Akita, M. Haruta, H. Sakurai, Q. Xu, Au@ZIF-8: CO Oxidation over Gold Nanoparticles Deposited to Metal-Organic Framework, J. Am. Chem. Soc. 131 (2009) 11302–11303.

[18] D. Esken, S. Turner, O.I. Lebedev, G. Van Tendeloo, R.A. Fischer, Au@ZIFs: Stabilization and Encapsulation of Cavity-Size Matching Gold Clusters inside Functionalized Zeolite Imidazolate Frameworks ZIFs, Chem. Mater. 22 (2010) 6393–6401.

[19] B. Volosskiy, K. Niwa, Y. Chen, Z. Zhao, N.O. Weiss, X. Zhong, M. Ding, C. Lee, Y. Huang, X. Duan, Metal-Organic Framework Templated Synthesis of Ultrathin, Well-Aligned Metallic Nanowires, ACS Nano 9 (2015) 3044–3049.

[20] J. Ke, W. Su, S.M. Howdle, M.W. George, D. Cook, M. Perdjon-Abel, P.N. Bartlett, W. Zhang, F. Cheng, W. Levason, G. Reid, J. Hyde, J. Wilson, D.C. Smith, K. Mallik, P. Sazio, Electrodeposition of metals from supercritical fluids, PNAS 106 (2009) 14768–14772.

[21] M.S. Sander, L.S. Tan, Nanoparticle arrays on surfaces fabricated using anodic alumina films as templates, Adv. Funct. Mater. 13 (2003) 393–397.

[22] D.H. Wang, W.L. Zhou, B.F. McCaughy, J.E. Hampsey, X.L. Ji, Y.B. Jiang, H.F. Xu, J. K. Tang, R.H. Schmehl, C. O'Connor, C.J. Brinker, Y.F. Lu, Electrodeposition of metallic nanowire thin films using mesoporous silica templates, Adv. Mater. 15 (2003) 130–133.

[23] A. Keilbach, J. Moses, R. Koehn, M. Doeblinger, T. Bein, Electrodeposition of Copper and Silver Nanowires in Hierarchical Mesoporous Silica/Anodic Alumina Nanostructures, Chem. Mater. 22 (2010) 5430–5436.

[24] S. Senthilkumar, A. Adisa, R. Saraswathi, R.A.W. Dryfe, Electrodeposition within zeolite membrane hosts, Electrochem. Commun. 10 (2008) 141–145.

[25] R. Ameloot, L. Stappers, J. Fransaer, L. Alaerts, B.F. Sels, D.E. De Vos, Patterned Growth of Metal-Organic Framework Coatings by Electrochemical Synthesis, Chem. Mater. 21 (2009) 2580–2582.

[26] B. Van de Voorde, R. Ameloot, I. Stassen, M. Everaert, D. De Vos, J.-C. Tan, Mechanical properties of electrochemically synthesised metal-organic framework thin films, J. Mater. Chem. C 1 (2013) 7716–7724.

[27] N. Campagnol, T. Van Assche, T. Boudewijns, J. Denayer, K. Binnemans, D. De Vos, J. Fransaer, High pressure, high temperature electrochemical synthesis of metal-organic frameworks: films of MIL-100 (Fe) and HKUST-1 in different morphologies, J. Mater. Chem. A 1 (2013) 5827–5830.

[28] S. Yadnum, J. Roche, E. Lebraud, P. Négrier, P. Garrigue, D. Bradshaw, C. Warakulwit, J. Limtrakul, A. Kuhn, Site-Selective Synthesis of Janus-type Metal-Organic Framework Composites, Angew. Chem. Int. Ed. 126 (2014) 4082–4086.

[29] I. Stassen, M. Styles, T. Van Assche, N. Campagnol, J. Fransaer, J. Denayer, J.-C. Tan, P. Falcaro, D. De Vos, R. Ameloot, Electrochemical Film Deposition of the Zirconium Metal–Organic Framework UiO-66 and Application in a Miniaturized Sorbent Trap, Chem. Mater. 27 (2015) 1801–1807.

[30] S.D. Worrall, H. Mann, A. Rogers, M.A. Bissett, M.P. Attfield, R.A.W. Dryfe, Electrochemical deposition of zeolitic imidazolate framework electrode coatings for supercapacitor electrodes, Electrochim. Acta 197 (2016) 228–240.

[31] S.S.Y. Chui, S.M.F. Lo, J.P.H. Charmant, A.G. Orpen, I.D. Williams, A chemically functionalizable nanoporous material Cu₃(TMA)₂(H₂O)₃, Science 283 (1999) 1148–1150.

metal electrodeposition in Cu/MOF, Electrochem. Commun. 8 (2006) 1830–1834.

[32] J. Getzschmann, I. Senkovska, D. Wallacher, M. Tovar, D. Fairen-Jimenez, T. Düren, J.M. van Baten, R. Krishna, S. Kaskel, Methane storage mechanism in the metal-organic framework $Cu_3(btc)_2$: An in situ neutron diffraction study, Micropor. Mesopor. Mater. 136 (2010) 50–58.

[33] M.D. Allendorf, R.J.T. Houk, L. Andruszkiewicz, A.A. Talin, J. Pikarsky, A. Choudhury, K.A. Gall, P.J. Hesketh, Stress-induced Chemical Detection Using Flexible Metal-Organic Frameworks, J. Am. Chem. Soc. 130 (2008) 14404–14405.

[34] K.T. Butler, C.H. Hendon, A. Walsh, Electronic Structure Modulation of Metal–Organic Frameworks for Hybrid Devices, ACS Appl. Mater. Interfaces 6 (2014) 22044–22050.

[35] M. Meilikhov, K. Yusenko, D. Esken, S. Turner, G. Van Tendeloo, R.A. Fischer, Metals@MOFs — Loading MOFs with Metal Nanoparticles for Hybrid Functions, Eur. J. Inorg. Chem. (2010) 3701–3714.

[36] J. Gubicza, J.L. Lábár, L.M. Quynh, N.H. Nam, N.H. Luong, Evolution of size and shape of gold nanoparticles during long-time aging, Mater. Chem. Phys. 138 (2013) 449–453.

[37] K. Sugikawa, Y. Furukawa, K. Sada, SERS-Active Metal–Organic Frameworks Embedding Gold Nanorods, Chem. Mater. 23 (2011) 3132–3134.

[38] L. He, Y. Liu, J. Liu, Y. Xiong, J. Zheng, Y. Liu, Z. Tang, Core–Shell Noble-Metal@Metal-Organic-Framework Nanoparticles with Highly Selective Sensing Property, Angew. Chem. Int. Ed. 52 (2013) 3741–3745.

[39] M.C. Dixon, T.A. Daniel, M. Hieda, D.M. Smilgies, M.H.W. Chan, D.L. Allara, Preparation, structure, and optical properties of nanoporous gold thin films, Langmuir 23 (2007) 2414–2422.

[40] M. Iosin, P. Baldeck, S. Astilean, Study of trptophan assisted synthesis of gold nanoparticles by combining UV-Vis, fluuoresence, and SERS spectroscopy, J. Nanopart. Res. 12 (2010) 2843–2849.

[41] S.L. Cheng, M.F. Chen, Fabrication, characterization, and kinetic study of vertical single-crystalline CuO nanowires on Si substrates, Nanoscale Res. Lett. 7 (2012) 1–9.